



Cite this: DOI: 10.1039/d0nj03578e

# Selective hydrogenation of cinnamaldehyde over magnetic flower-like carbonaceous Pd catalysts†

 Dan Zhang,<sup>a</sup> BOWEI Wang,<sup>id</sup> \*<sup>abc</sup> Lijuan Yan,<sup>a</sup> Ruixiao Gao,<sup>a</sup> Lu Liu,<sup>a</sup> Ziyi Xia,<sup>a</sup> Xilong Yan,<sup>id</sup> \*<sup>abc</sup> Yang Li,<sup>id</sup> \*<sup>abc</sup> and Ligong Chen<sup>id</sup> <sup>abc</sup>

Synthesis of an easily separable and efficient catalyst is of great significance for selective hydrogenation of unsaturated functional groups. In this work, novel magnetic flower-like carbonaceous Pd catalysts are constructed for the selective reduction of the C=C bond. According to the characterization results, a flower-like architecture is observed in the catalysts containing both Fe<sub>3</sub>O<sub>4</sub> and Pd NPs, which is constructed by the secondary self-assembly in the preparation process due to the interaction between Pd and magnetic nitrogen-doped graphene (Fe<sub>3</sub>O<sub>4</sub>-NG). More flower-like structures are formed by increasing the Pd loading amount, further enhancing the specific surface area of the catalyst. The specific surface area of Pd-FONG-3 is the highest (521.17 m<sup>2</sup> g<sup>-1</sup>). Combining the results of characterization and experiments, it is found that the catalytic activity is positively related to the flower-like architecture and the interaction between Pd NPs (6.0 nm) and Fe<sub>3</sub>O<sub>4</sub> NPs (6.7 nm). Fe<sub>3</sub>O<sub>4</sub> is not only beneficial to the magnetic recovery of the catalyst, but also acts as a cocatalyst, which can significantly improve the reactant conversion. Moreover, N species play an important role in protecting the C=O bond, resulting in the selective hydrogenation of the C=C group. Herein, Pd-FONG-3 exhibits excellent activity in the selective hydrogenation of cinnamaldehyde (CAL) with 99.5% conversion and 96.5% hydrocinnamaldehyde (HCAL) selectivity, and its catalytic performance is much better than that of the commercial 5% Pd/C catalyst (100% conversion and 69.1% HCAL selectivity). This work provides a new strategy to construct highly active catalysts with magnetic recovery properties for selective hydrogenation of C=C bonds, and Pd-FONG-3 shows tremendous application foreground.

 Received 16th July 2020,  
 Accepted 3rd November 2020

DOI: 10.1039/d0nj03578e

[rsc.li/njc](http://rsc.li/njc)

## Introduction

Catalytic hydrogenation is extremely attractive due to the high atom utilization of H<sub>2</sub> and eco-friendliness. Cinnamaldehyde (CAL), as a typical  $\alpha,\beta$ -unsaturated aldehyde, plays a significant role in the industrial and academic application, such as the synthesis of flavors, pharmaceuticals and paints.<sup>1–4</sup> Since CAL has three unsaturated functional groups, namely phenyl, C=C bond and aldehyde groups, study on selective hydrogenation of CAL becomes particularly important. Hydrocinnamaldehyde (HCAL), cinnamyl alcohol (COL) and hydrocinnamyl alcohol (HCOL) can be obtained by hydrogenation of C=C bonds and/or C=O bonds (Scheme 1). Among them, the product HCAL obtained by hydrogenation of C=C bonds is stable in

alkaline medium, and can be used as a blending soap essence or correcting agent in various flavors. Therefore, it is necessary to find a catalyst that can selectively conduct the hydrogenation of C=C bonds. These catalysts mainly include homogeneous and heterogeneous catalysts. Homogeneous catalysts, which have sufficient contact with the substrate, can achieve the efficient reaction results, but there are also some difficulties in after-treatment.<sup>5</sup> Nevertheless, heterogeneous catalysts are widely used in catalytic reactions due to the mild reaction conditions and simple separation process.

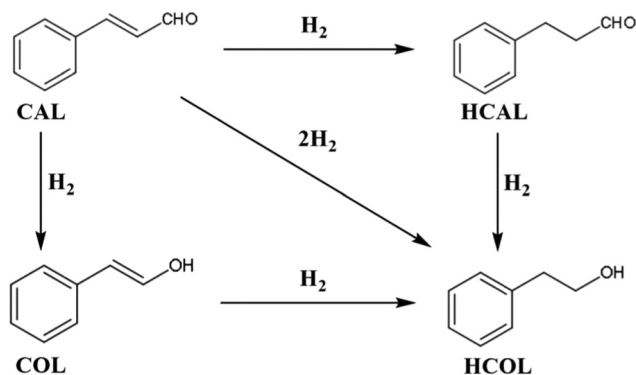
It is crucial to develop highly effective and high selectivity heterogeneous catalysts for hydrogenation of C=C bonds in CAL. Palladium is one of the most widely reported metals used in the hydrogenation of the C=C bond.<sup>6–11</sup> For instance, palladium on activated carbon (Pd/AC) is a traditional catalyst for selective hydrogenation of  $\alpha,\beta$ -unsaturated aldehydes.<sup>12</sup> However, most of this catalyst is recovered by filtration, which is not economical and environmentally friendly. The most effective method is to develop magnetic catalysts that can be easily separated from the reaction system for recycling.<sup>13–16</sup> Moreover, the magnetically separable nature of the catalyst could aid in reducing the operational energy and time. For example,

<sup>a</sup> School of Chemical Engineering and Technology, Tianjin University, Tianjin 300350, P. R. China. E-mail: bwwang@tju.edu.cn, yan@tju.edu.cn, liyang777@tju.edu.cn

<sup>b</sup> Collaborative Innovation Center of Chemical Science and Engineering (Tianjin), Tianjin 300072, P. R. China

<sup>c</sup> Tianjin Engineering Research Center of Functional Fine Chemicals, Tianjin, P. R. China

† Electronic supplementary information (ESI) available. See DOI: 10.1039/d0nj03578e



Scheme 1 Catalytic hydrogenation of CAL.

Hyeon *et al.*<sup>15</sup> reported a simple gram-scale synthesis of Pd-Fe<sub>3</sub>O<sub>4</sub> heterodimer nanocrystals, which exhibited good activities for Suzuki coupling reactions. This nanocrystal catalyst could be easily separated from the reaction mixture due to its ferromagnetism. Zhu *et al.*<sup>16</sup> presented Fe<sub>3</sub>O<sub>4</sub>@MOF core-shell magnetic microspheres as excellent catalysts for the Claisen-Schmidt condensation reaction. Remarkably, it can be easily separated and recycled without significant loss of catalytic efficiency. Nemati *et al.*<sup>17</sup> successfully synthesized magnetic mesoporous polymelamine formaldehyde nanocomposite-incorporating ZnO NPs by solvothermal and sol-gel methods, which can be easily separated from the reaction medium and reused without significant changes in catalytic activity. Among them, the introduction of magnetic materials is the most attractive and straightforward method. Another drawback is the instability of Pd/AC after several cycles due to detrimental aggregation and leaching of Pd NPs.<sup>18</sup> Shao *et al.*<sup>19</sup> developed the core-shell nanocatalyst ZIF-8@Pd@MOF-74 for the preferential reduction of C=C groups. However, the catalytic activity of ZIF-8@Pd@MOF-74 decreased remarkably when the number of cycles increased. Furthermore, one problem of these catalysts is that only part of the active sites on the surface of the catalyst acted, and the efficiency was still expected to increase. It is not hard to see that studies on the Pd-based catalysts are also very active due to the interfacial interactions which have a large effect on the catalyst activity.<sup>20–25</sup>

In our previous report, magnetic 3D nitrogen doped graphene gels were synthesized for the reduction of 4-nitrophenol to 4-aminophenol.<sup>26</sup> Compared to the traditional catalyst supports, graphene offers higher activity and selectivity with a large specific surface area, high-speed electron mobility, good electrical conductivity, *etc.*<sup>27–33</sup> Modification of graphene can lead to obtaining more excellent materials, in which doped nitrogen regulate the activity and dispersion of supported metals to some extent.<sup>34–38</sup> Therefore, in this work, we tried to construct an efficient, environmentally friendly and magnetically recoverable Pd catalyst to solve the above-mentioned problems. A series of Pd catalysts supported by magnetic nitrogen doped graphene gels were prepared and applied for the selective hydrogenation of CAL. Characterization methods were employed to study the structure-activity relationship of the catalysts.<sup>39</sup> The results indicated that a flower-like architecture

was constructed *via* self-assembly in the Pd loading process, which led to the large surface area of the catalyst and further enhanced the catalytic activity. As an affordable co-catalyst, Fe<sub>3</sub>O<sub>4</sub> NPs on nitrogen doped graphene gels exhibited a positive influence on the activity. Doped N species were also beneficial to the selective reduction of C=C bonds. Moreover, the reaction parameters and the reusability of the catalyst were investigated in detail.

## Experimental

### Materials

Except for special instructions, all reagents and chemicals were of analytical grade and used without further purification. Graphite powder was purchased from Tianjin Guangfu Technology Development Co. Ltd, Tianjin, China. FeCl<sub>3</sub>·6H<sub>2</sub>O was purchased from Tianjin Standard Technologies Co., Ltd, Tianjin, China. FeCl<sub>2</sub>·4H<sub>2</sub>O was purchased from Tianjin Fengchuan Chemical Reagent Technologies Co., Ltd, Tianjin, China. PdCl<sub>2</sub> was purchased from Sinopharm Chemical Reagents Beijing Co., Ltd, Beijing, China. CAL (GC) was purchased from Shanghai Aladdin Bio-Chem Technology Co., Ltd, Shanghai, China.

### Preparation of GO, Fe<sub>3</sub>O<sub>4</sub>-NG and NRG

Graphene oxide (GO) was prepared by the oxidation of graphite according to the Hummers' method.<sup>40</sup> According to the report, magnetic nitrogen-doped graphene (Fe<sub>3</sub>O<sub>4</sub>-NG) was synthesized by the hydrothermal method.<sup>26</sup> 2 mL aqueous solution of FeCl<sub>3</sub>·6H<sub>2</sub>O (0.081 g) and FeCl<sub>2</sub>·4H<sub>2</sub>O (0.030 g) was added into 50 mL GO aqueous dispersion (2 mg mL<sup>-1</sup>). After 20 minutes of ultrasonication, 10 mL of ethylenediamine was added to the mixture. And then the mixture was poured into a 100 mL Teflon-lined autoclave and kept it for 12 hours at 180 °C. After cooling to room temperature, the obtained gel was washed with deionized water to pH ≈ 7 and freeze-dried. N-doped reduced graphene oxides (NG) were also prepared which used 2 mL of water replacing the solution of FeCl<sub>3</sub>·6H<sub>2</sub>O and FeCl<sub>2</sub>·4H<sub>2</sub>O.

### Preparation of Pd-FONG-1.5, Pd-FONG-3 and Pd-NG-3

The catalysts were prepared by the sodium borohydride reduction method. After being ground into powder, Fe<sub>3</sub>O<sub>4</sub>-NG (270 mg) was added to 45 mL of deionized water and stirred. Then, ammonia solution of PdCl<sub>2</sub> was added dropwise into the mixture and stirred for 40 min. Excess sodium borohydride solution (0.1 M) was slowly added dropwise into the mixture and stirred for 3 h. The mixture was filtered, and then washed with deionized water several times to remove the residual chlorine and boron-containing ions. Meanwhile, the solution of silver nitrate was added dropwise into the water that was used to wash the filter cake until no precipitation formed to ensure the elimination of chloride ions. Furthermore, ICP-OES and EDS were employed to confirm the disappearance of B and Cl. Finally, after vacuum drying, the obtained solid was ground to fine powder. The obtained solid powder was named Pd-FONG-X,

where X represents the load of Pd (wt%). Besides, Pd-NG-3 was fabricated by a similar process in which NG was used as the support.

### Characterization

X-ray diffraction (XRD) patterns were obtained by using a BRUKER AXS GMBH D8-Focus with a Cu-K $\alpha$  X-ray source in the range of 5–80°. Scanning electron microscopy (SEM) was performed on a Hitachi S-4800 microscope. Transmission electron microscopy (TEM) images were recorded *via* a JEOL JEM-2100F microscope. Scanning transmission electron microscopy (STEM) images were recorded by using an energy dispersive spectrometer (EDS; EDAX PV6761/55). Elemental analysis was carried out using an inductar EL cube elemental analyzer and inductively coupled plasma optical emission spectrometry (ICP-OES) was performed by using a Vista-MPX spectrometer. The specific surface area was determined by the Brunauer–Emmer–Teller (BET) method with nitrogen physisorption at a liquid nitrogen temperature on a NOVA 2000e analyzer (Quantachrome, U.S.A.). The X-ray photoelectron spectroscopy (XPS) measurements were carried out on an EscaLab Xi+ spectrometer.

### Liquid-phase hydrogenation of CAL

The hydrogenation reaction took place in an autoclave with 15 mL Teflon lining. A stirrer, catalyst (0.25 mmol% Pd), solvent (3 mL), and CAL (2 mmol) in turn were added to the autoclave. Before starting the reaction, the autoclave should be slowly purged at least 7 times with N<sub>2</sub> and H<sub>2</sub>, respectively, to remove air, and then pressurized to 2 MPa H<sub>2</sub>. And then, the autoclave was placed in a preheating oil bath with magnetic stirring and kept there for a certain time. The reactants were analyzed by using a gas-chromatogram with an AT-OV-101 capillary column using a flame ionization detector.

### Reusability of Pd-FONG-3

For the catalyst reusability test, the reaction conditions were 2 mmol CAL, 18 mg Pd-FONG-3 (0.25 mmol% Pd), 3 mL toluene, 80 °C, 2 MPa H<sub>2</sub>, 1.5 h. All reactions were conducted in an autoclave according to the procedures described above. Due to the magnetism of Pd-FONG-3, the used catalyst was easily separated by a magnet, washed with toluene, dried, and then reused under the same experimental conditions. The reusability of the catalyst was evaluated by the value of  $C_n/C_1$  and  $S_n/S_1$  ( $n = 2, 3, 4, \text{ and } 5$ ).  $C_1$  is the conversion of CAL in the first run, while  $C_n$  is the conversion of CAL in the  $n$  cycle. Analogously,  $S_1$  represents the selectivity of HCAL in the first run, while  $S_n$  is the selectivity of HCAL in the  $n$  cycle.

## Results and discussion

### Catalyst characterization

Fig. 1 shows the XRD patterns of GO, NG, Pd-NG-3, Fe<sub>3</sub>O<sub>4</sub>-NG, Pd-FONG-1.5 and Pd-FONG-3, respectively. The obvious diffraction peak at 11.9° was assigned to the GO, confirming the

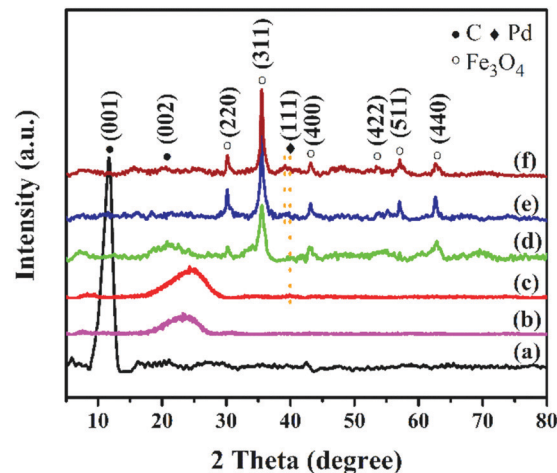


Fig. 1 XRD patterns of (a) GO, (b) NRGO, (c) Pd-NG-3, (d) Fe<sub>3</sub>O<sub>4</sub>-NG, (e) Pd-FONG-1.5 and (f) Pd-FONG-3.

successful synthesis of GO (Fig. 1a).<sup>41,42</sup> The broad peak of NG at 24.3° belonged to the diffraction peak of the C (002) crystal faces with an interlayer spacing of 0.37 nm, and the GO standard peak disappeared due to the total reduction of GO (Fig. 1b).<sup>36,43</sup> The corresponding peaks of Fe<sub>3</sub>O<sub>4</sub>-NG, Pd-FONG-1.5 and Pd-FONG-3 were at about 22.2° and an interlayer spacing was about 0.42 nm (Fig. 1d–f), which increased obviously, probably because Fe<sub>3</sub>O<sub>4</sub> NPs hindered the stacking of carbon layers.<sup>26</sup> In the curves of Fe<sub>3</sub>O<sub>4</sub>-NG, Pd-FONG-1.5 and Pd-FONG-3, diffraction peaks at 30.1°, 35.5°, 43.0°, 53.3°, 57.0° and 62.6° can be found, which can be indexed to the (220), (311), (400), (422), (511) and (440) crystal faces of Fe<sub>3</sub>O<sub>4</sub> (Fig. 1d–f).<sup>44,45</sup> Moreover, the Pd(111) crystal face diffraction peak in Pd-NG-3 was identified at 39.9° with a lattice spacing of 0.226 nm.<sup>31,44</sup> However, the Pd standard peak shifted to 39.5° in Pd-FONG-1.5 with a lattice spacing of 0.228 nm, and to 39.1° in Pd-FONG-3 with a lattice spacing of 0.230 nm, which proved that the interaction might be created *via* Pd NPs and Fe<sub>3</sub>O<sub>4</sub> NPs.<sup>21–23</sup>

Fig. 2 shows the SEM images of Fe<sub>3</sub>O<sub>4</sub>-NG, Pd-FONG-1.5, Pd-FONG-3 and Pd-NG-3. From Fig. 2a, a rich pore structure of Fe<sub>3</sub>O<sub>4</sub>-NG is observed owing to the self-assembly in the hydrothermal process. A few flower-like architectures with petals composed of thin layers were found from Pd-FONG-1.5 (Fig. 2b) and there were more flower-like architectures in Pd-FONG-3 (Fig. 2c). The flower-like architecture could also be observed in STEM images (Fig. S2, ESI<sup>†</sup>). This architecture was possibly constructed by the secondary self-assembly in the preparation process due to the interaction between Pd and Fe<sub>3</sub>O<sub>4</sub>-NG. Similar structures were also reported by some studies, which can increase the specific surface area of the material.<sup>36,46–50</sup> The results of the BET test also verified that the specific surface area of Pd-FONG-3 is the highest (521.17 m<sup>2</sup> g<sup>−1</sup>) (Table 1). Pd-NG-3 consisted of a mesh channel structure (the lowest specific surface area, 311.74 m<sup>2</sup> g<sup>−1</sup>) (Table 1).

TEM images of Fe<sub>3</sub>O<sub>4</sub>-NG, Pd-FONG-1.5, Pd-FONG-3 and Pd-NG-3 are presented in Fig. 3. From all images, it can be

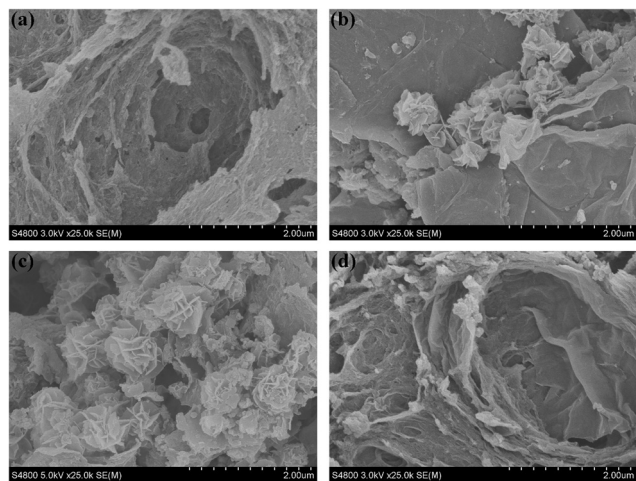


Fig. 2 The SEM images of (a)  $\text{Fe}_3\text{O}_4$ -NG, (b) Pd-FONG-1.5, (c) Pd-FONG-3 and (d) Pd-NG-3.

Table 1 Physical and textural properties of different catalysts

Catalyst	Mass concentration				$S_{\text{BET}}$ ( $\text{m}^2 \text{g}^{-1}$ )	$V_{\text{total}}$ ( $\text{cm}^3 \text{g}^{-1}$ )	$D_{\text{average}}$ (nm)
	$\text{C}^a$	$\text{N}^a$	$\text{H}^a$	$\text{Pd}^b$			
NRGO	75.38	9.77	2.42	—	—	—	—
$\text{Fe}_3\text{O}_4$ -NG <sup>c</sup>	44.37	5.50	2.30	—	24.04	312.33	0.29
Pd-NG-3	71.37	9.14	2.21	2.44	—	311.74	0.25
Pd-FONG-1.5	48.96	5.84	1.73	1.26	26.49	394.67	0.43
Pd-FONG-3	42.36	4.92	2.42	2.79	24.95	521.17	0.59

<sup>a</sup> Mass concentration was detected in elemental analysis. <sup>b</sup> Mass concentration was measured by ICP-OES. <sup>c</sup> The BET test was carried out after being ground into powder.

observed that NPs were uniformly dispersed on the supports. In the TEM image of Pd-FONG-3, Pd NPs and  $\text{Fe}_3\text{O}_4$  NPs were observed clearly; the addition of Fe species did not affect the dispersion of Pd NPs. The average particles sizes of four catalysts are shown in Fig. 3. The average particle size of  $\text{Fe}_3\text{O}_4$  NPs in  $\text{Fe}_3\text{O}_4$ -NG was about 6.7 nm, and the average particle size of NPs in Pd-FONG-1.5 and Pd-FONG-3 was about 8.2 nm and 8.1 nm, respectively, but it was hard to distinguish Pd and  $\text{Fe}_3\text{O}_4$  NPs strictly. It was found that the introduced Pd species could increase the  $\text{Fe}_3\text{O}_4$  NP size slightly. Moreover, in Pd-NG-3, the average particle size of Pd NPs was about 6.0 nm. Fig. 3 shows the STEM images of Pd-FONG-3, from which it can be observed that this catalyst contained C, N, O, Fe and Pd elements. Evidently, Pd NPs distributed around  $\text{Fe}_3\text{O}_4$  NPs which indicated that the formation of Pd NPs was related to  $\text{Fe}_3\text{O}_4$  NPs.

Moreover, the elemental contents of the prepared catalysts are also listed in Table 1. According to the results of elemental analysis and ICP-OES test, the contents of N in the catalysts were 9.77%, 5.50%, 9.14%, 5.84% and 4.92%, respectively. As expected, the Pd content of Pd-FONG-3 was twice as that of Pd-FONG-1.5, and it was also consistent with the theoretical value.

The analyses of surface composition and valence state were carried out by using XPS measurements and the results are

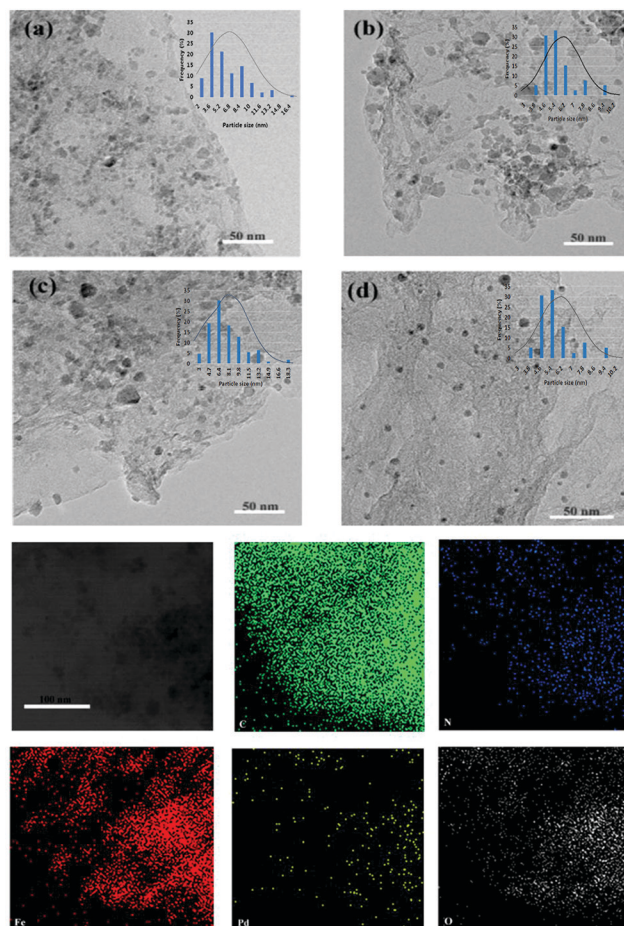


Fig. 3 TEM images and particle size distribution histograms of (a)  $\text{Fe}_3\text{O}_4$ -NG, (b) Pd-FONG-1.5, (c) Pd-FONG-3, (d) Pd-NG-3 and STEM images of Pd-FONG-3.

presented in Fig. 4. Fig. 4a shows the wide scan spectra of the five samples. The binding energy peaks at about 284.5 eV, 399.2 eV and 531.3 eV were attributed to C 1s, N 1s and O 1s, respectively.<sup>26,31,39</sup> The N 1s spectra of  $\text{Fe}_3\text{O}_4$ -NG, Pd-FONG-3 and Pd-NG-3 revealed that N species have four forms including pyridinic-N, amine-N, pyrrolic-N and graphitic-N at about 398.2 eV, 399.2 eV, 400.0 eV, and 400.9 eV (Fig. 4b-d).<sup>55</sup> Pyridinic-N and amine-N were dominant in the three catalysts (Table S1, ESI<sup>†</sup>). XPS analysis also provided the state of the Pd 3d region (Fig. 4e). The two peaks with binding energies of about 335.0 eV (Pd  $3d_{5/2}$ ) and 340.3 eV (Pd  $3d_{3/2}$ ) confirmed the presence of metallic Pd<sup>0</sup> in the catalyst and this result was in line with the XRD characterization. Compared with the Pd  $3d_{5/2}$  binding energy peak of Pd-NG-3 at 335.0 eV, the Pd  $3d_{5/2}$  peaks of Pd-FONG-1.5 and Pd-FONG-3 shifted to a higher value (335.3 eV), which were possibly affected by  $\text{Fe}_3\text{O}_4$  NPs, indicating again that the interaction was generated between Pd NPs and  $\text{Fe}_3\text{O}_4$  NPs. The interaction between them resulted in the redistribution of charge and affected the binding energy. And a lower binding energy indicates that Pd on the surface of Pd-NG-3 possessed a reduction (electron gain) state and weak adsorbate binding energies.<sup>51–53</sup> The Fe  $2p_{3/2}$  binding energy

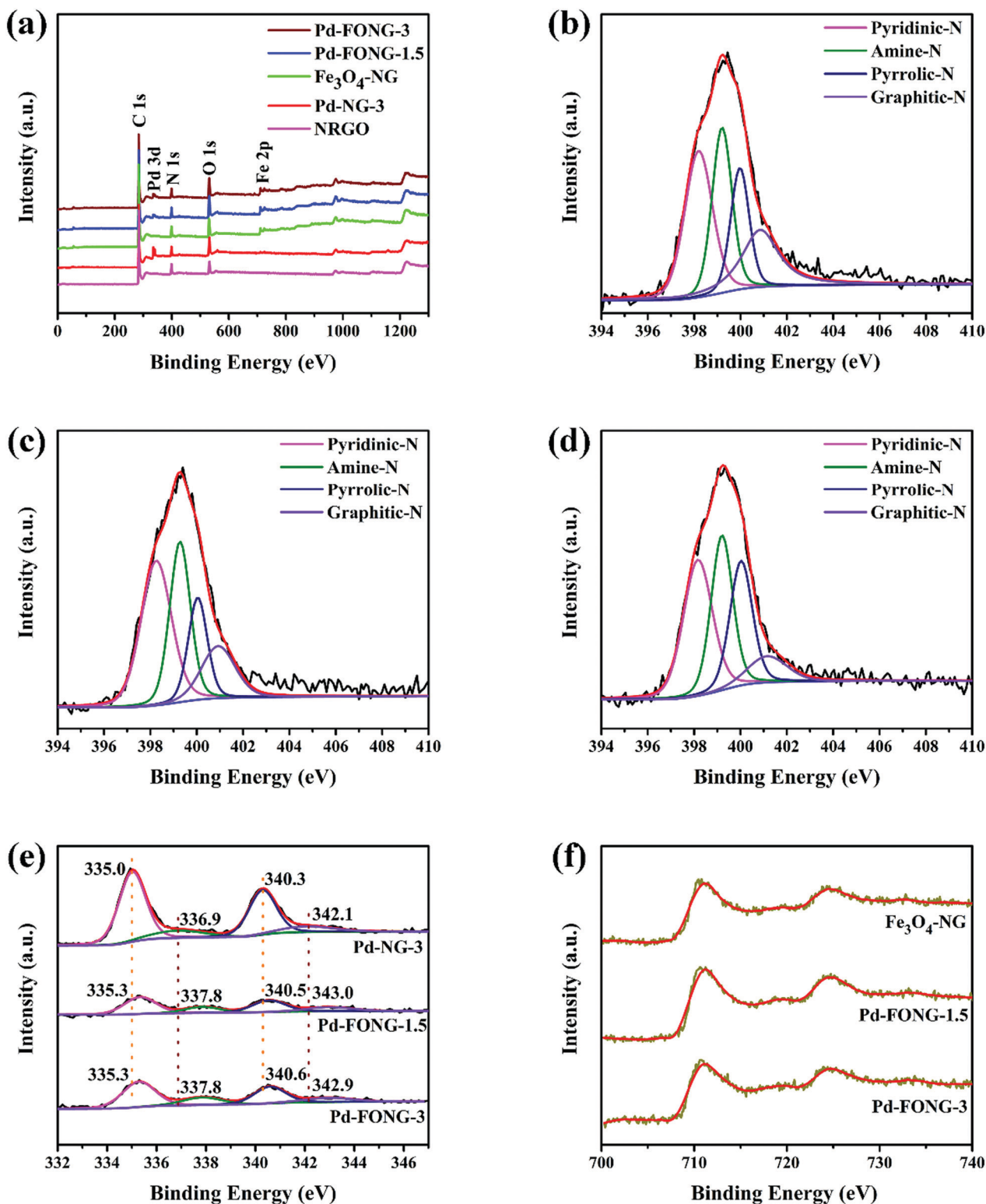


Fig. 4 (a) XPS survey spectra of NRGO, Pd-NG-3, Fe<sub>3</sub>O<sub>4</sub>-NG, Pd-FONG-1.5, and Pd-FONG-3, N1s spectra of (b) Fe<sub>3</sub>O<sub>4</sub>-NG, (c) Pd-FONG-3 and (d) Pd-NG-3, (e) Pd 3d spectra of Pd-NG-3, Pd-FONG-1.5 and Pd-FONG-3, (f) Fe 2p spectra of Fe<sub>3</sub>O<sub>4</sub>-NG, Pd-FONG-1.5 and Pd-FONG-3.

peak was at about  $711.2 \pm 0.2$  eV, and the Fe  $2p_{1/2}$  binding energy peak was at  $724.5 \pm 0.2$  eV (Fig. 4f),<sup>54</sup> further confirming the presence of Fe<sub>3</sub>O<sub>4</sub> NPs. The binding energy of the Fe  $p_{3/2}$

peak in Pd-FONG-1.5 and Pd-FONG-3 was slightly lower than that in Fe<sub>3</sub>O<sub>4</sub>-NG, further confirming the interaction between Pd and Fe<sub>3</sub>O<sub>4</sub> NPs.

Table 2 Hydrogenation of CAL over different catalysts<sup>a</sup>

Entry	Catalysts	Conversion (%)	Selectivity (%)		
			HCAL	COL	HCOL
1	Pd-NG-3	8.1 ± 0.43	84.9 ± 0.29	—	15.1 ± 0.74
2	Pd-FONG-1.5	88.0 ± 0.10	89.2 ± 0.08	—	10.8 ± 0.15
3	Pd-FONG-3	86.7 ± 0.12	92.4 ± 0.04	—	7.6 ± 0.26
4	Fe <sub>3</sub> O <sub>4</sub> -NG <sup>b</sup>	—	—	—	—
5	Pd/C	100.0	69.1 ± 0.58	—	30.9 ± 0.73

<sup>a</sup> Reaction conditions: 2 mmol CAL, catalyst (0.25 mmol% Pd, catalyst dosage was calculated by the amount of active metal Pd, and the Pd content is 0.25 mmol% of CAL), 3 mL toluene, 70 °C, 2 MPa H<sub>2</sub>, 2 h. <sup>b</sup> Amount: 18 mg.

### Catalytic performance

Hydrogenation of CAL over the above-mentioned catalysts was carried out to evaluate the catalytic performance and the results are shown in Table 2. Pd-NG-3, a Fe<sub>3</sub>O<sub>4</sub>-free catalyst, was hard to catalyze the reaction along with only 8.1% conversion (entry 1). However, Pd-FONG-3 gave the excellent conversion (86.7%, entry 3) under the same conditions, indicating that Fe<sub>3</sub>O<sub>4</sub> NPs had a great influence on the reaction. Meanwhile, when the content of Pd in the catalyst decreased, Pd-FONG-1.5 afforded 88.0% conversion and 89.2% selectivity of HCAL (entry 2), the selectivity of the catalyst had decreased. This may be due to the larger specific surface area in Pd-FONG-3 provided by the flower-like architecture (Fig. 2 and Table 1). Notably, Pd-FONG-3 contained more pyridinic nitrogen, and the ratio of pyridinic-N to pyrrolic-N was the highest. This

Table 3 Conversion and selectivity data in the different solvents<sup>a</sup>

Entry	Solvent	Conversion (%)	Selectivity (%)	
			HCAL	HCOL
1	Water	24.5 ± 0.25	82.5 ± 0.13	17.5 ± 0.30
2	Cyclohexane	64.7 ± 0.68	90.8 ± 0.28	9.2 ± 0.50
3	Ethanol	38.8 ± 0.77	91.7 ± 0.62	8.3 ± 0.65
4	Toluene	86.7 ± 0.11	92.4 ± 0.07	7.6 ± 0.35
5	Ethyl acetate	8.2 ± 0.49	93.1 ± 0.54	6.9 ± 0.40

<sup>a</sup> Reaction conditions: 2 mmol CAL, Pd-FONG-3 (0.25 mmol% Pd), 3 mL solvent, 70 °C, 2 MPa H<sub>2</sub>, 2 h.

beneficial effect of pyridinic-N was explained *via* a more facile heterolytic activation of molecular hydrogen. Fe<sub>3</sub>O<sub>4</sub>-NG, however, had no activity on the reaction which implied that Fe<sub>3</sub>O<sub>4</sub> NPs only played an auxiliary role (entry 4). Compared to commercial Pd/C (entry 5), Pd-FONG-3 exhibited a higher selectivity to HCAL. That might be the influence of N species on support, which could keep the C=O groups away from Pd, and then inhibit further hydrogenation of HALD.<sup>55</sup> Therefore, the outstanding results of Pd-FONG-3 may be caused by the co-catalyst Fe<sub>3</sub>O<sub>4</sub> and flower-like N doped graphene support.

In order to optimize the conversion of CAL and the selectivity of HCAL, some factors influencing the reaction were explored, such as solvent media, reaction temperature, H<sub>2</sub> pressure and reaction time.

Table 3 shows the results of catalytic hydrogenation of CAL over Pd-FONG-3 in different solvent media. The highest conversion of CAL was obtained with toluene as the solvent (86.7%, entry 4).

The influence of reaction temperature on hydrogenation of CAL to HCAL over Pd-FONG-3 was investigated in the range of 60–100 °C (Fig. 5a). The increase of the hydrogenation temperature favored the conversion of CAL, which increased from 53.1% (60 °C) to 99.5% (80 °C). The selectivity of HCAL also increased significantly to 96.5%. As the temperature continued to increase, CAL completely reacted, but the selectivity of HCAL decreased to 91.4% at 100 °C. Thus, the optimum reaction temperature was 80 °C.

According to Fig. 5b, the influence of H<sub>2</sub> pressure on hydrogenation of CAL to HCAL over Pd-FONG-3 could be figured out in the scope of 1–3 MPa. When the H<sub>2</sub> pressure was from 1 MPa to 2 MPa, the conversion of CAL increased gradually by 11.8% to 99.5%. As the pressure continued to increase to 3 MPa, the conversion was almost unchanged, but the selectivity of HCAL decreased to 91.8%. Obviously, 2 MPa of H<sub>2</sub> pressure can lead to higher conversion and selectivity.

Fig. 5c shows the fluctuation of the conversion and selectivity data with the change of reaction time. The conversion grew sharply by 77.1% to 99.5% when the reaction time was extended from 0.5 h to 2 h. On continuing the extension of the reaction time, CAL was completely converted. With the change

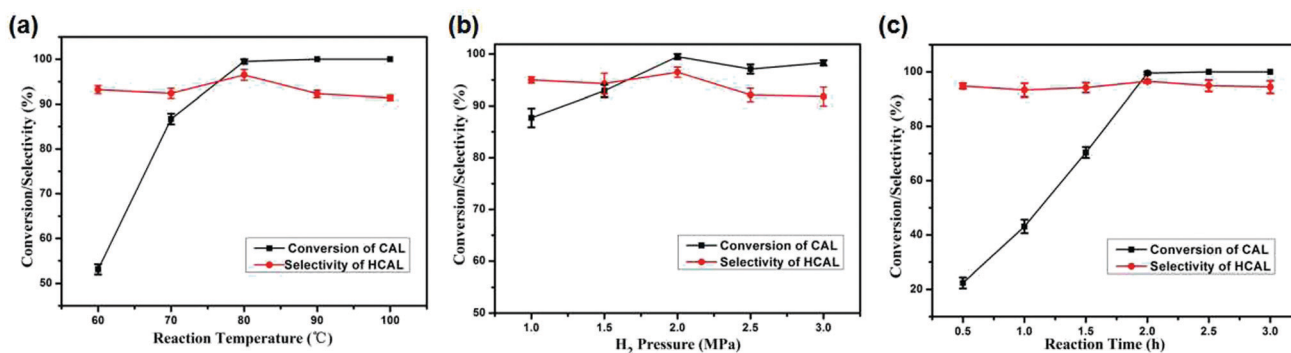


Fig. 5 Effects of reaction temperature (other conditions: 2 mmol CAL, Pd-FONG-3 (0.25 mmol% Pd), 3 mL toluene, 2 MPa H<sub>2</sub>, 2 h), H<sub>2</sub> pressure (other conditions: 2 mmol CAL, Pd-FONG-3 (0.25 mmol% Pd), 3 mL toluene, 80 °C, 2 h) and reaction time (other conditions: 2 mmol CAL, Pd-FONG-3 (0.25 mmol% Pd), 3 mL toluene, 80 °C, 2 MPa H<sub>2</sub>) over Pd-FONG-3.

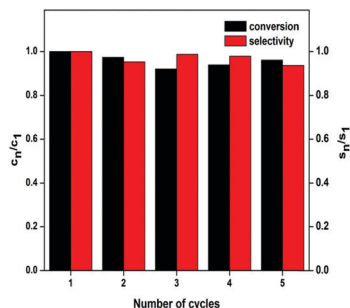


Fig. 6 Reusability test of Pd-FONG-3 for hydrogenation of CAL. Reaction conditions: 2 mmol CAL, 18 mg Pd-FONG-3 (0.25 mmol% Pd), 3 mL toluene, 80 °C, 2 MPa H<sub>2</sub>, 1.5 h.

of reaction time, the selectivity remained stable at about 95% and reached the maximum of 96.5% at 2 h. This also alluded to the difficulty of C=O bond reduction.<sup>56</sup> At the same time, considering the energy saving, two hours was chosen as the best reaction time with 99.5% of conversion and 96.5% of selectivity.

By exploring a series of parameters, 99.5% of conversion and 96.5% of selectivity as the optical reaction results were obtained over Pd-FONG-3 under the conditions: solvent, 3 mL toluene; reaction temperature, 80 °C; H<sub>2</sub> pressure, 2 MPa; reaction time, 2 h.

### Reusability of Pd-FONG-3

It is well known that the reusability of the catalyst is also very important.<sup>57</sup> According to Fig. 6, it was found that the CAL conversion and HCAL selectivity fluctuated slightly in the following 4 cycles and the CAL conversion and HCAL selectivity were still higher than 90% and 95% of the first run, respectively. The results proved that Pd-FONG-3 exhibited good reusability for at least 5 cycles.

## Conclusion

In summary, we have successfully fabricated a series of Pd catalysts supported by magnetic nitrogen doped graphene gels including Pd-NG-3, Pd-FONG-1.5 and Pd-FONG-3 for hydrogenation of CAL. Among them, the addition of Fe<sub>3</sub>O<sub>4</sub> was not only beneficial to the magnetic recovery of the catalysts, but also Fe<sub>3</sub>O<sub>4</sub> acted as a cocatalyst, which could significantly improve the conversion of CAL. Meanwhile, Fe<sub>3</sub>O<sub>4</sub> NPs affected the formation of Pd NPs to a certain extent. The interlayer spacing and binding energy of Pd NPs in Pd-FONG-1.5 and Pd-FONG-3 had changed compared to that in Pd-NG-3. Moreover, the flower-like architecture in Pd-FONG-1.5 and Pd-FONG-3 increased the specific surface area. Among all the catalysts, Pd-FONG-3 presented the best performance and attained 99.5% conversion of CAL and 96.5% selectivity of HCAL after investigating the effects of some factors.

## Conflicts of interest

There are no conflicts to declare.

## Acknowledgements

This project is funded by the National Natural Science Foundation of China (Grant No. 21808161 and 21978208) and China Postdoctoral Science Foundation (Grant No. 2020T130465).

## References

- B. Bachiller-Baeza, I. Rodriguez-Ramos and A. Guerrero-Ruiz, *Appl. Catal., A*, 2001, **205**, 227.
- J. Zhao, J. Ni, J. Xu, J. Xu, J. Cen and X. Li, *Catal. Commun.*, 2014, **54**, 72.
- M. Zhao, K. Yuan, Y. Wang, G. Li, J. Guo, L. Gu, W. Hu, H. Zhao and Z. Tang, *Nature*, 2016, **539**, 76.
- Y. Yang, D. Rao, Y. Chen, S. Dong, B. Wang, X. Zhang and M. Wei, *ACS Catal.*, 2018, **8**, 11749.
- I. Szatmari, G. Papp, F. Joo and A. Katho, *Inorg. Chim. Acta*, 2018, **472**, 302.
- S. Chen, L. Meng, B. Chen, W. Chen, X. Duan, X. Huang, B. Zhang, H. Fu and Y. Wan, *ACS Catal.*, 2017, **7**, 2074.
- X. Chen, H. Cao, X. Chen, Y. Du, J. Qi, J. Luo, M. Armbruster and C. Liang, *ACS Appl. Mater. Interfaces*, 2020, **12**, 18551.
- S. Bewana, M. J. Ndolomingo, E. Carleschi, B. P. Doyle, R. Meijboom and N. Bingwa, *ACS Appl. Mater. Interfaces*, 2019, **11**, 32994.
- R. Paul, C. Sarkar, Y. Yan, Q. T. Trinh, B. S. Rao, C.-W. Pao, J.-F. Lee, W. Liu and J. Mondal, *ChemCatChem*, 2020, **12**, 3687.
- I. Szewczyk, R. Kosydar, P. Natkanski, D. Duraczynska, J. Gurgul, P. Kustrowski and A. Drelinkiewicz, *J. Porous Mater.*, 2020, **27**, 1287.
- F. Wang, Y. Bi, K. Hu and X. Wei, *Chem. – Eur. J.*, 2020, **26**, 4874.
- F. Zhao, Y. Ikushima, M. Chatterjee, M. Shirai and M. Arai, *Green Chem.*, 2003, **5**, 76.
- Y. Jia, H. Ma, W. Zhang, G. Zhu, W. Yang, N. Son, M. Kang and C. Liu, *Chem. Eng. J.*, 2020, 383.
- F.-A. Khan and G. Suess-Fink, *Eur. J. Inorg. Chem.*, 2012, 727.
- Y. Jang, J. Chung, S. Kim, S. W. Jun, B. H. Kim, D. W. Lee, B. M. Kim and T. Hyeon, *Phys. Chem. Chem. Phys.*, 2011, **13**, 2512.
- F. Ke, L.-G. Qiu and J. Zhu, *Nanoscale*, 2014, **6**, 1596.
- Z. Shahamat, F. Nemati and A. Elhampour, *Mol. Diversity*, 2020, **24**, 691.
- F. Zhao, Y. Ikushima, M. Chatterjee, M. Shirai and M. Arai, *Green Chem.*, 2003, **5**, 76.
- C. Guo, C. Liang, X. Qin, Y. Gu, P. Gao, M. Shao and W.-T. Wong, *ACS Appl. Nano Mater.*, 2020, **3**, 7242.
- S. Chen, L. Meng, B. Chen, W. Chen, X. Duan, X. Huang, B. Zhang, H. Fu and Y. Wan, *ACS Catal.*, 2017, **7**, 2074.
- R. Li, W. Yao, Y. Jin, W. Jia, X. Chen, J. Chen, J. Zheng, Y. Hu, D. Han and J. Zhao, *Chem. Eng. J.*, 2018, **351**, 995.
- M. Kolodziej, A. Drelinkiewicz, E. Lalik, J. Gurgul, D. Duraczynska and R. Kosydar, *Appl. Catal., A*, 2016, **515**, 60.

- 23 Q. Fu, W.-X. Li, Y. Yao, H. Liu, H.-Y. Su, D. Ma, X.-K. Gu, L. Chen, Z. Wang, H. Zhang, B. Wang and X. Bao, *Science*, 2010, **328**, 1141.
- 24 C. Wang, H. Daimon and S. Sun, *Nano Lett.*, 2009, **9**, 1493.
- 25 X. Sun, S. Guo, Y. Liu and S. Sun, *Nano Lett.*, 2012, **12**, 4859.
- 26 B. Wang, L. Si, J. Geng, Y. Su, Y. Li, X. Yan and L. Chen, *Appl. Catal., B*, 2017, **204**, 316.
- 27 Z. Weng and F. Zaera, *ACS Catal.*, 2018, **8**, 8513.
- 28 L. Q. Zhang, J. M. Winterbottom, A. P. Boyes and S. Raymahasay, *J. Chem. Technol. Biotechnol.*, 1998, **72**, 264.
- 29 B. Coq, V. Brotons, J. M. Planeix, L. C. de Menorval and R. Dutartre, *J. Catal.*, 1998, **176**, 358.
- 30 T.-H. Tri, K. Chizari, I. Janowska, M. S. Moldovan, O. Ersen, L. D. Nguyen, M. J. Ledoux, P.-H. Cuong and D. Begin, *Catal. Today*, 2012, **189**, 77.
- 31 R. Nie, M. Miao, W. Du, J. Shi, Y. Liu and Z. Hou, *Appl. Catal., B*, 2016, **180**, 607.
- 32 A. R. Siamaki, A. E. R. S. Khder, V. Abdelsayed, M. S. El-Shall and B. F. Gupton, *J. Catal.*, 2011, **279**, 1.
- 33 G. M. Scheuermann, L. Rumi, P. Steurer, W. Bannwarth and R. Muelhaupt, *J. Am. Chem. Soc.*, 2009, **131**, 8262.
- 34 K.-J. Jeon, Z. Lee, E. Pollak, L. Moreschini, A. Bostwick, C.-M. Park, R. Mendelsberg, V. Radmilovic, R. Kostecki, T. J. Richardson and E. Rotenberg, *ACS Nano*, 2011, **5**, 1042.
- 35 S. Ramakrishnan, M. Karuppanan, M. Vinothkannan, K. Ramachandran, O. J. Kwon and D. J. Yoo, *ACS Appl. Mater. Interfaces*, 2019, **11**, 12504.
- 36 J. Yao, K. Zhang, W. Wang, X. Zuo, Q. Yang, H. Tang, M. Wu and G. Li, *ACS Appl. Mater. Interfaces*, 2018, **10**, 19564.
- 37 Y. Gao, G. Hu, J. Zhong, Z. Shi, Y. Zhu, D. S. Su, J. Wang, X. Bao and D. Ma, *Angew. Chem., Int. Ed.*, 2013, **52**, 2109.
- 38 H. Wang, X. Feng, M. Zhou, X. Bo and L. Guo, *ACS Appl. Nano Mater.*, 2020, **3**, 6336.
- 39 Y. Dong and X. Fei, *Mater. Technol.*, 2020, **35**, 102.
- 40 W. Hummers, Jr. and R. Offeman, Preparation of graphitic oxide, *J. Am. Chem. Soc.*, 1958, **80**, 1339.
- 41 H. Hu, Z. Zhao, W. Wan, Y. Gogotsi and J. Qiu, *Adv. Mater.*, 2013, **25**, 2219.
- 42 J. Geng, L. Si, H. Guo, C. Lin, Y. Xi, Y. Li, X. Yan, B. Wang and L. Chen, *New J. Chem.*, 2017, **41**, 15447.
- 43 L. Guo, P. Ye, J. Wang, F. Fu and Z. Wu, *J. Hazard. Mater.*, 2015, **298**, 28.
- 44 S. J. Hoseini, V. Heidari and H. Nasrabadi, *J. Mol. Catal. A: Chem.*, 2015, **396**, 90.
- 45 X. Lin, X. Wang, Q. Zhou, C. Wen, S. Su, J. Xiang, P. Cheng, X. Hu, Y. Li, X. Wang, X. Gao, R. Nozel, G. Zhou, Z. Zhang and J. Liu, *ACS Sustainable Chem. Eng.*, 2019, **7**, 1673.
- 46 Y. Ma, J. Huang, L. Lin, Q. Xie, M. Yan, B. Qu, L. Wang, L. Mai and D.-L. Peng, *J. Power Sources*, 2017, **356**, 98.
- 47 X. Hou, J. Liu, W. Guo, S. Li, Y. Guo, Y. Shi and C. Zhang, *Catal. Commun.*, 2019, **121**, 27.
- 48 X. Lin, X. Wang, Q. Zhou, C. Wen, S. Su, J. Xiang, P. Cheng, X. Hu, Y. Li, X. Wang, X. Gao, R. Nozel, G. Zhou, Z. Zhang and J. Liu, *ACS Sustainable Chem. Eng.*, 2019, **7**, 1673.
- 49 L. Hou, L. Lian, L. Zhang, G. Pang, C. Yuan and X. Zhang, *Adv. Funct. Mater.*, 2015, **25**, 238.
- 50 C. Wu, X. Huang, G. Wang, L. Lv, G. Chen, G. Li and P. Jiang, *Adv. Funct. Mater.*, 2013, **23**, 506.
- 51 S.-F. Jiang, L.-L. Ling, Z. Xu, W.-J. Liu and H. Jiang, *Ind. Eng. Chem. Res.*, 2018, **57**, 13055.
- 52 H. A. Elazab, A. R. Siamaki, S. Moussa, B. F. Gupton and M. S. El-Shall, *Appl. Catal., A*, 2015, **497**, 58.
- 53 I. E. L. Stephens, A. S. Bondarenko, U. Gronbjerg, J. Rossmeisl and I. Chorkendorff, *Energy Environ. Sci.*, 2012, **5**, 6744.
- 54 M. Qiao, X. Lei, Y. Ma, L. Tian, X. He, K. Su and Q. Zhang, *Nano Res.*, 2018, **11**, 1500.
- 55 S. Patchkovskii, J. S. Tse, S. N. Yurchenko, L. Zhechkov, T. Heine and G. Seifert, *Proc. Natl. Acad. Sci. U. S. A.*, 2005, **102**, 10439.
- 56 F. Jiang, J. Cai, B. Liu, Y. Xu and X. Liu, *RSC Adv.*, 2016, **6**, 75541.
- 57 S. L. Scott, *ACS Catal.*, 2018, **8**, 8597.